BACHELOR'S THESIS / BIOMEDICAL ENGINEERING 2022

Electrophysiological model of the left ventricle: prediction of reentry circuits with fast simulations based on cellular automata applying clinical stimulation protocols

Paula Franco Ocaña

upf. Universitat Pompeu Fabra Barcelona

Electrophysiological model of the left ventricle: prediction of reentry circuits with fast simulations based on cellular automata applying clinical stimulation protocols

Paula Franco Ocaña

Bachelor's Thesis UPF 2021/2022

Thesis Supervisor(s):

Pr. Oscar Camara , (Department of Information and Communication Technologies (DTIC))

Acknowledgments

Behind this Bachelor Thesis there are many people who have helped and supported me throughout the journey. Foremost, I would like to express my gratitude to my supervisor, Oscar Camara, for all his professional guidance and constructive recommendations. I would also want to express my sincere gratitude towards the CoMMLab research group, specially to Dolors and Pau, for their help, assistance and contributions in the project. I also need to thank the people who are part of Dr. Antonio Berruezo's team in the arrhythmia unit at *Centro Médico Teknon*. Thanks to the doctors, engineers and nurses I have been working with over the last year, I have learned a lot from all of you. Concretely, thanks to David and Dani for their help and guidance. I also have to thank my friends for their support and wise advice, not only in the project, but throughout the last five years. Finally, I owe my profound gratitude to my family, Jose, Merche, Claudia and Samuel, for their unconditional love, support and constant encouragement during these years.

Thank you.

Summary/Abstract

Myocardial infarction (MI) is a common cardiovascular disease that causes irreversible damage to the left ventricle (LV) myocardium, resulting in the formation of scar tissue. When this phenomenon occurs, reentry circuits appear, generating alternative conduction channels. This is associated with an increased risk of developing ventricular arrhythmias and consequently, sudden cardiac death. Patient-specific 3D computational modelling and simulations can be used to predict non-invasively the reentry circuits causing ventricular tachycardia (VT). Cellular automata (CA) electrophysiological models allow to reproduce VT while performing simulations near real-time, overcoming the computational burden limitations of biophysical models. The aim of the present study was to create computational cardiac models capable of stratifying VT inducibility in infarcted patients by virtually applying the real pacing protocol followed in the clinic using a novel CA-based solver developed at *Universitat de València*, in which no real clinical data has been tested yet. 3D computational LV and biventricular models were obtained from cardiac magnetic resonance images provided by *Centro Médico Teknon*, allowing to identify the scar configuration and arrhythmogenic substrate of each patient. The models were reconstructed to fit in the CA, and seven pacing sites were defined to apply the virtual pacing protocol. The obtained in-silico simulations results were compared with the actual results obtained by patients during an electrophysiological study (EPS). The similarity of the results between in-silico and EPS demonstrated that the novel CA-based fast electrophysiological simulator together with the implementation of real pacing protocols were valid for assessing VT risk in infarcted patients.

Keywords

Electrophysiological simulations; cardiac modelling; cellular automata; myocardial infarction; ventricular tachycardia; clinical pacing protocols.

Preface or prologue

During the past year, I have been doing an internship in the arrhythmia and electrophysiology unit at *Centro Médico Teknon*. Initially, my intention was to apply the knowledge acquired in the different subjects of the Biomedical Engineering degree and to learn how engineers worked in the clinical environment. However, during the course of the internship, my interest in electrophysiology arose. By seeing how important the role of engineers was during the interventions, and by taking part in different research projects, I knew that I wanted my Bachelor Thesis to be related to electrophysiology and computational modelling. Thanks to my stay in the electrophysiology unit, I have been able to have a more clinical and engineering vision of the concepts that I wanted to develop, being able to combine the knowledge from the clinical point of view and from the computational one, as there is not always a close link between the two. This Bachelor Thesis allowed me to deepen my knowledge in computational cardiac models and to develop a work that, if followed, could have an impact in the future. Hence, this work aims to contribute to the development of computational ventricular arrhythmia predictive models by making them clinically specialized, to eventually be as reliable as the procedures performed in the clinical practice.

Index

List of Figures

List of Tables

1 Introduction

1.1 Clinical background

Sudden cardiac death (SCD) is one of the major causes of worldwide mortality and it is responsible for nearly half of all deaths from cardiovascular diseases [1, 2]. Nevertheless, in the past 20 years, cardiovascular mortality has decreased in high-income countries in response to the adoption of preventive measures to reduce the burden of heart failure [3]. However, the prediction of SCD is one of the most challenging fields in arrhythmology and the attempts to provide reliable indicators of SCD have driven one of the most active areas of research in arrhythmology over the past decades [4].

SCD causes approximately 4,000,000 deaths per year [5], and a large proportion of these result from ventricular arrhythmias (VA), being patients who have suffered a myocardial infarction (MI) at a higher risk of developing them [3, 5]. VA are a type of arrhythmias that originate in the ventricles. They can be divided mainly in two types: ventricular tachycardia (VT) and ventricular fibrillation (VF). VT is characterized by a rapid and regular heartbeat (<100 beats/minute) that prevents the ventricles from fully contracting, causing less blood to be pumped to the body. On the other hand, VF is a severely abnormal rapid heartbeat that causes the ventricles to quiver, provoking collapse and cardiac arrest [6]. As previously mentioned, the probability of suffering from VA increases in post-MI patients. MI causes irreversible damage to the myocardium, resulting in the formation of scar tissue in the left ventricle (LV). This scar tissue is characterized by a reduction of blood flow in that specific area, leading to myocardial cell death and thus affecting the contractile function of the LV [7, 8]. Since this tissue is no longer excitable, electrical propagation is also altered, preventing proper propagation of the electrical impulse.

Figure 1 represents the normal electrical activity of the heart, where the sinoatrial node (SAN) is the primary pacemaker, responsible for generating the impulse. Then, the impulse is conducted via the atrial myocardium towards the atrioventricular node (AVN). From the AVN the electrical impulse is rapidly transmitted toward the His bundle (HB) that divides in left and right branches. Finally, the electrical impulse reaches the ventricular myocardium through the Purkinje fibers to ensure a coordinated activation of the ventricular myocardium [9]. However, when scar tissue is present in the LV, as it acts as an anatomical barrier for electrical impulse to propagate, reentry circuits may appear, leading to VA [10].

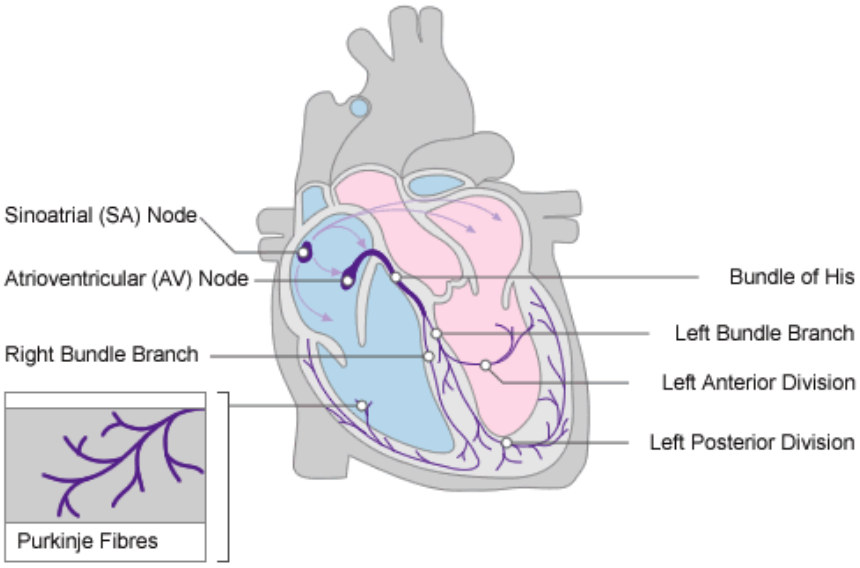

Figure 1: Electrical conduction system of the heart. Image obtained from: *University of Nottingham.*

A reentry arrhythmia is a cardiac rhythm abnormality in which the action potential (AP) propagates similar to a closed-loop circuit [10, 11]. Under normal conditions, the electrical impulse finishes when all fibers have depolarized and are completely refractory. Nevertheless, if an isolated group of fibers has not been activated during the initial depolarization wave, these fibers may be excited before the impulse is extinguished, because they still have time to depolarize. They can act then as a link to re-excite previously depolarized areas that have been recovered from the initial depolarization [12, 13].

The post-infarct LV scar has a heterogeneous geometry, and is characterized by three distinct regions: the healthy myocardial tissue, the core zone (CZ) and the border zone (BZ). The CZ corresponds to the diseased tissue that has lost its electrical properties, and the BZ to the area of viable myocardium adjacent to the core zone. This region presents altered electrical activation properties, as fibrotic zones intersect with myocytes [14], thus provoking alternative conduction channels (CC), as represented in Figure 2. The structural and electrical remodeling in the infarct BZ can result in slow conduction, increasing the probability of reentry circuits appearance. Alternative CCs within the scar act as VT isthmuses and correlate with the slow conduction channels, constituting the arrhythmogenic substrate [15, 16].

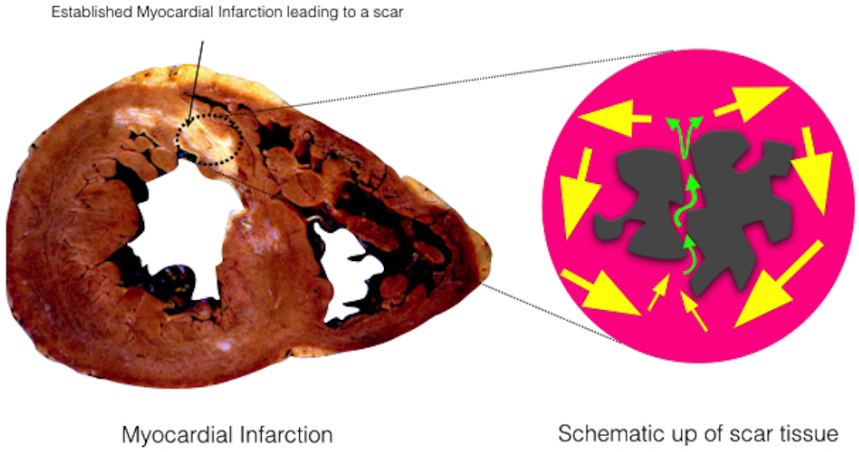

Figure 2: Left image: Transversal plane of an infarcted left ventricle. Enhanced white region corresponds to scar tissue. *Right image*: Representation of a reentry circuit. Pink region: Border zone, Gray region: Core zone, Yellow arrows: reentry pathway, Green arrows: slow conduction channel. Image obtained from: *Melbourne Heart Rhythm.*

Nowadays, the only indicator that has consistently shown a relation with increased risk of SCD in the setting of MI and left ventricular dysfunction is the left ventricle ejection fraction (LVEF) [17]. This variable has been used for more than a decade to guide the use of an implantable cardioverter defibrillator (ICD) for primary prevention of SCD. If the LVEF is below 35%, an ICD will be implanted, even if patients do not present arrhythmogenic substrate. Nevertheless, LVEF is not an accurate and highly reproducible clinical parameter [3]. While ICDs can effectively terminate VT in patients with ischemic or non-ischemic cardiomyopathy, they may not prevent arrhythmia recurrence [18].

A radiofrequency ablation (RFA) procedure is considered the default surgical intervention to treat VTs. This intervention consists of applying radiofrequency energy to specific areas of the diseased myocardium. The local delivery of energy causes an increase in temperature in the abnormal tissue resulting in tissue injury and thus, eliminating the source of VA. RFA is a common procedure to isolate reentry pathways across the infarct scar that are responsible for VT [19].

However, prior to RFA, patients must undergo an electrophysiological study (EPS). This procedure is performed to detect whether patients have inducible VT. During the EPS, a catheter is placed in the right ventricle (RV) apex, which is stimulated with a specific pacing protocol to detect whether patients have inducible VT or not [20]. In addition, patients may also present clinical VTs, which are those that are registered on a device: a Holter monitor, pacemaker, ICD or cardiac resynchronization therapy device. In the case of inducible or clinical VT, the physician will proceed to study whether VT ablation is necessary.

The identification of VT sources of origin during the procedure is difficult. Therefore, during RFA, characterization of the arrhythmogenic substrate is performed by a process called electro-anatomical mapping (EAM). The objective of acquiring an EAM is to obtain an activation map of the cardiac structure in order to identify the site of abnormal electrical signals [21]. This EAM is usually guided by the *CARTO* System (Biosense Webster, Diamond Bar, CA), which is a software used for 3D mapping in electrophysiology procedures, even though other navigation softwares are also used such as *EnSite NavX* (St. Jude Medical, Austin, TX) or *LocaLisa* (Medtronic, Minneapolis, MN). The *CARTO* electro-anatomical system uses an integrated catheter with a localization sensor embedded in the distal part to enable automatic and simultaneous acquisition of the electrogram in that position, thus being able to reconstruct a 3D-electro-anatomical map of the LV [19].

Despite the reconstruction generated during the procedure, EAM only provides information about endocardial and epicardial surfaces, not providing an accurate reconstruction of the heart anatomy. Therefore, in advanced electrophysiology units, they perform image-guided RFA. In these interventions, they make use of pre-operative imaging to study myocardial tissue properties, such as the scar characteristics, for then being fused with EAM during the RFA in order to better guide the procedure. For image-guided VT ablation procedure, two main imaging modalities are used: cardiac magnetic resonance imaging (CMR) and computed tomography (CT). CMR combined with gadolinium, a contrast agent, allows an accurate identification and quantification of the infarcted tissue. This sequence is called late-gadolinium-enhanced CMR (LGE-CMRs) [22, 23, 24]. Contrast-enhanced CT (CE-CT) also allows for a clear identification of blood and myocardium [25]. Although CE-CT is not the main imaging technique used to treat VTs, it allows to distinguish the myocardial wall thickness, which has shown correlation with scar region and electrophysiological abnormalities [26].

Consequently, the use of medical imaging is a fundamental tool to complement and accelerate these interventions, since the information obtained from the images is crucial for the detection of scar tissue and arrhythmogenic substrate, and allows the clinical professionals to know with more precision where to ablate, making the intervention less tedious. In the work developed by Andreu et al. [27], instead of characterizing the arrhythmogenic substrate through an EAM, a previous analysis on the LGE-CMR is performed, whereby the scar tissue is analyzed. The scar characterization can be depicted as color-coded pixel-signal-intensity maps that have a reasonably high correlation with the EAMs obtained during the ablation procedures. This previous analysis allows to identify alternative CCs, which have been related to VT isthmuses in the EAM. Therefore, by knowing in advance the possible alternative CCs, it is not necessary to perform an EAM, and thus, reduce procedure time, since the ablation points will be applied where the software has detected. Figure 3 shows the LGE-CMR analysis prior to the procedure integrated in the *CARTO* system by which they guided the substrate VT ablation.

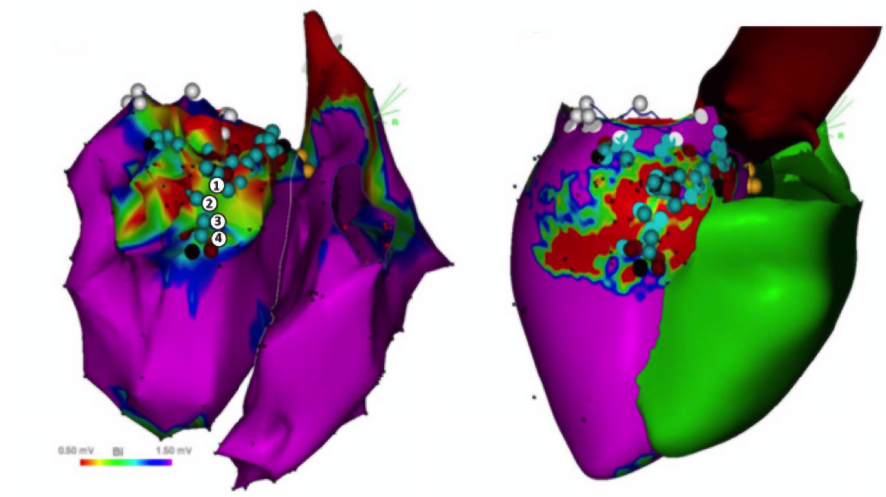

Figure 3: Integration of LGE-CMR information into the *CARTO3* navigation system. Inferior view of the left and right ventricles. *Left image*: Endocardial bipolar voltage EAM. Black dots: alternative CC entrance; Blue dots: inner CC; Red dots: RFA points. *Right image*: Signal intensity map obtained from LGE-CMR registered in the EAM. Red area: Core zone; Blue-Green-Yellow area: Border one; Purple area: Healthy tissue. LGE-CMR: Late-gadolinium-enhanced cardiac magnetic resonance; EAM: Electro-anatomical mapping. CC: conduction channel. RF: Radiofrequency ablation. Image obtained from: Andreu et al. (2017) [27].

However, although VT-RFA is the main technique of choice when treating infarct-related VT, it is considered challenging and time-consuming [19], and shows relatively low success, since almost 40% of patients that undergo this intervention have recurrent VT after the procedure [28]. Therefore, new approaches such as computational heart models, are being considered in relation to predicting the electrical behavior of the heart and providing additional insights to guide RFA procedures [29].

1.2 State of the art of computational heart models in post-myocardial infarction patients

Computational models in health care are increasing the capacity to diagnose and be determinant in the detection of certain pathologies. The 'Digital Twin' era, where the clinical data can be integrated in virtual models, is boosting. The main two pillars of 'Digital Twin' are the creation of mechanistic and statistical models. Mechanistic models provide better clinical interpretability and are able to make predictions, while statistical models are able to extract parameters and find new metrics from the data [30]. Computational cardiac models are an example of it, since they can be used as personalized and non-invasive arrhythmia predictors for post-infarct patients, while new parameters for analysis can be extracted.

The principal steps when creating virtual heart models for VT applications are: the acquisition of patient-specific images, the segmentation and labeling of the LV cardiac tissue (CZ, BZ and healthy tissue), the construction of the 3D geometry, the incorporation of fiber orientation and the assignment of electrophysiological

properties in each region (epicardium, endocardium and mid-myocardium) at a cell and tissue level. Then, pacing protocols are applied to induce VT in the virtual heart. The outcome of these virtual electrophysiological studies can be used to predict the arrhythmia risk of a post-MI patient [31].

In the last decade, intensive research in the field of computational cardiac electrophysiology has demonstrated the ability of three-dimensional cardiac computational models to perform in-silico electrophysiological studies. Trayanova et al. [29] established the Virtual-heart Arrhythmia Risk Predictor (VARP) approach, where they demonstrated that VARP outperformed clinical metrics (such as the LVEF) in predicting future arrhythmic events. Moreover, scar characterization by a previous analysis in LGE-CMR has demonstrated that a significant scar mass ($<5\%$) and scar characteristics are related with VA, being able to stratify arrhythmogenic risk [32, 33]. With this non-invasive approaches, SCD could be prevented and avoid unnecessary ICD implantations in post-infarction patients.

In the study by López-Pérez et al. [28], from computational heart models they were able to induce clinical VT of a patient with infarct-related VT from different pacing points, identifying the slow conduction channels originating such VTs. However, although these models were very accurate, they were highly computationally expensive, requiring several hours per simulation and thus being difficult to integrate them in the timings of a clinical workflow.

Novel studies include machine learning (ML) algorithms in virtual heart simulations in order to better understand the disease and improve VA risk stratification [34]. Furthermore, new studies applying deep learning (DL) are increasingly being used to improve and optimize treatments such as for atrial fibrillation [35]. Also, the integration of ECG data to cardiac computational models is becoming more important, since ECG patterns may indicate if there is underlying abnormal electrical activity related to the VAs [36]. Although these current studies are not yet fully related to VTs, the integration of ECG to the heart model could be highly useful for VT risk prediction in the near future.

1.3 Electrophysiological models

Previous studies [28, 31] have embedded detailed cellular electrophysiological models of ventricular myocytes in their heart models. Hodgkin-Huxley formulations are the most typically used [37], but also, some of the most common human ventricular myocyte models used are the Ten Tusscher-Panfilov [38] and the O'Hara-Rudy [39]. In these models, membrane dynamics are modeled as an RC circuit where the resistances represent the ion flux through the membrane channels and the capacitor represents the cell membrane phospholipid bilayer. Based on this representation, complex ordinary differential and algebraic equations are defined to explain the behavior of myocyte cells as a function of the ionic currents in each element of the cardiac mesh [40].

To model electrophysiological cellular dynamics, different electrical propagation softwares are available. ELVIRA [41] and Alya [42] softwares apply finite element methods to simulate cardiac electrical propagation, and open source cardiac electrophysiology softwares such as OpenCARP [43], are also able to describe cardiac behavior at multi-scale level. To simulate the AP propagation, these softwares include biophysical models, making the simulations realistic and including detailed information of cellular dynamics. Nevertheless, as mentioned above, having highly-detailed electrophysiological models also entails a very high computational burden, making these detailed models unusable for processing a vast amount of cases and hampering clinical translation of the tools.

In order to overcome this drawback, other techniques such as cellular automata (CA) seem more appropriate. CA is a rule-based model based on volume discretization. It simplifies cardiac tissue by defining a finite number of defined states to each cell: resting, excited and refractory. Cells evolve in parallel at discrete time steps, following state update functions or dynamical transition rules, taking into account the neighbors cell states [44]. CA is a relatively simple and a low computational model, being useful if rapid simulations are needed. Although they are not as detailed as biophysical models, it has been demonstrated that with the correct input parameters, CA is able to reproduce reentrant VA from clinical data [45].

A novel CA-based software, *Arritmic3D*, has been developed by Serra et al. [46], with the aim of simulating and assessing arrhythmia risk in three-dimensional ventricular models by performing fast simulations. Compared to a biophysical solver, a 1200ms simulation took 7h, while with the CA took 76s. However, in *Arritmic3D* no real VT data or pacing protocols from specialized electrophysiological units have been tested yet. Nonetheless, this novel solver is of great interest as with the use of fast automata-based tools these simulations could finally be performed near real-time, making it compatible to the clinical setting.

1.4 Objectives

The main aim of this project was to create computational cardiac models capable of stratifying VT risk in patients with heterogeneous scar due to MI. Hence, the objectives were divided in the following way:

(i) Create fifteen LV patient-specific models from CMR images.
(ii) Apply the actual clinical pacing protocol used at *Centro Médico Teknon*.
(iii) Perform simulations with *Arritmic3D*, a CA-based electrophysiological software.
(iv) Validate results with real data.

The clinical data were provided by the electrophysiology unit of *Centro Médico Teknon* in Barcelona, where I have been working as an engineer technician, being involved in the interventions to better understand how computational models can help clinicians and patient outcomes. Furthermore, this project was also carried out with *Universitat Pompeu Fabra* and with the CoMMLab research group at *Universitat de València*, since *Arritmic3D* was developed by them.

2 Methods

For this project, two different setups were tested: a first one, in which only the LV was considered for the simulations; and a second one, in which the RV was also included, creating a biventricular model. The followed pipeline is shown in Figure 4. First, LGE-CMR images of each patient were acquired. Then, from the CMR, the LV and RV were segmented by delimitating the endocardial and the epicardial walls. After the delimitation, the CZ, the BZ and the heathy tissue of the LV needed to be adjusted in order to obtain the information regarding the scar's distribution. For each patient, a three-dimensional model of the LV and the RV with the corresponding arrhythmogenic substrate was obtained. Then, from the segmentations, the models were reconstructed in order to fit the CA. To achieve this, the ventricular models were automatically discretized through a pre-processing tool with the aim of obtaining nodes that represent different portions of tissue. Fiber orientation and electrophysiological properties were included in this voxelization process. Once created the complete ventricular models, the simulation setup was defined by replicating a real pacing protocol used in the clinic, and determining different pacing site locations. With that, *Arritmic3D* was used to virtually simulate and assess arrhythmia risk. Finally, the obtained in-silico simulations results were validated with the real data that patients obtained during their EPS. Moreover, scar metrics were extracted for evaluation of simulation's accuracy.

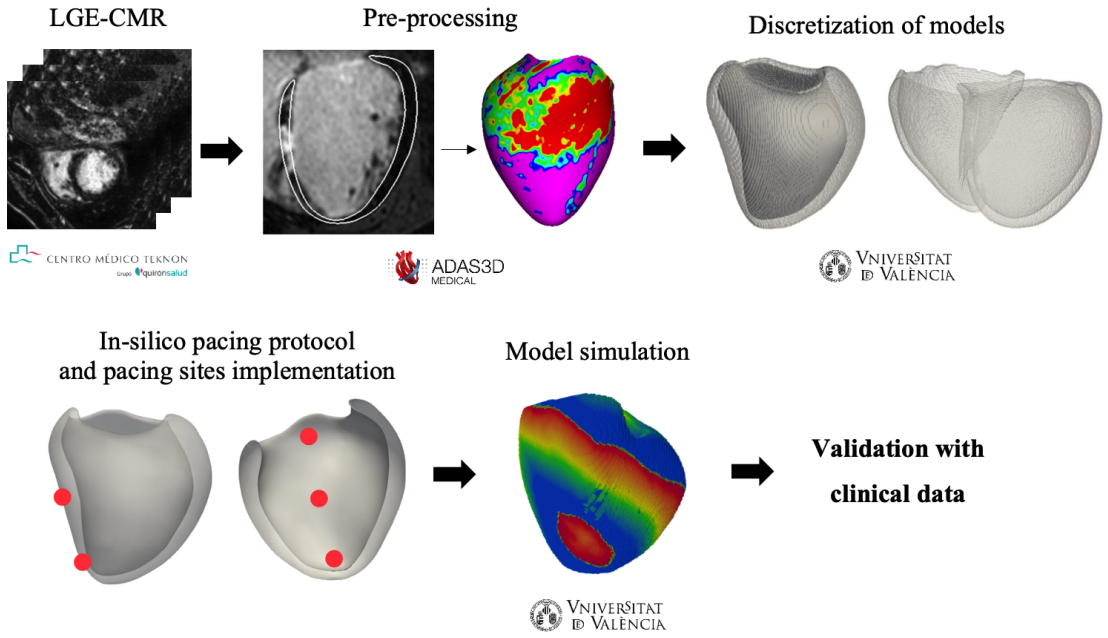

Figure 4: Pipeline followed to perform patient-specific fast simulations to determine the inducibility of VT in each patient. LGE-CMR: Late-gadolinium-enhanced cardiac magnetic resonance.

2.1 Data acquisition

The data used for the simulations were provided by the electrophysiology unit at *Centro Médico Teknon*, led by Dr. Antonio Berruezo. Patient data were extracted from a specific database of patients who had suffered a MI. The sample for this project was of 15 patients, each one of them having a heterogeneous scar in the LV due to a MI. The sample of patients was divided into three main groups, as shown in Figure 5: patients who had induced VT during an EPS, patients who did not have induced VT on the EPS, and patients who did not undergo an EPS. From this distribution, we could also differentiate those who also had clinical VT events and those who did not yet developed any VT episode.

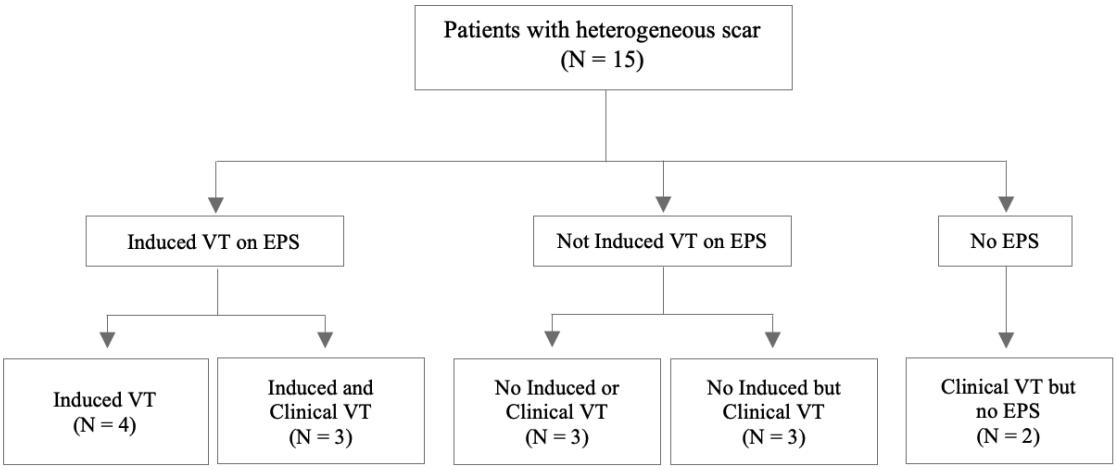

Figure 5: Division of patients based on whether they had induced or not VT episodes during an EPS. Subdivision of patients based on whether they had also clinical VT episodes.

The first step to perform the simulations was to obtain the CMR images of each patient. Image acquisition was performed using a 1.5-Tesla scanner (MAGNETOM TrioTM, Siemens Healthcare, Erlangen, Germany). Concretely, LGE-CMR images were needed in order identify the infarcted tissue. They were acquired in 120 slices with a spacing between slices of 1 mm and an isotropic resolution of 1 mm. LGE-CMR were 3D-DIXON type, since this sequence ensured adequate image acquisition and thus, a good characterization of the tissue.

2.2 Image pre-processing

Once acquired the LGE-CMRs, they were imported into *Adas3D* (Galgo Medical, Barcelona, Spain), a commercial image processing and 3D visualization software, which is specifically developed to process CMRs and provides information about fibrotic tissue. *Adas3D* was used in order to perform the segmentations of the LV and RV of each patient.

To obtain the LV segmentation, three steps needed to be carried out. The first step was to manually place four landmarks in the CMR: at the aortic annulus, at the mitral annulus, at the apex of the LV and at the tricuspid annulus. The second step consisted of manually delimitating the LV endocardium and epicardium in three randomly selected slices in the transversal plane: in the basal, mid and apical areas, respectively. From this delimitation, the software automatically delimitated the endocardium and epicardium. Finally, the third step consisted of a manual adjustment of the endocardial and epicardial walls. Figure 6 shows the endocardial and epicardial delimitation of the LV. Once these three main steps were performed, the software reconstructed automatically the 3D model of the LV.

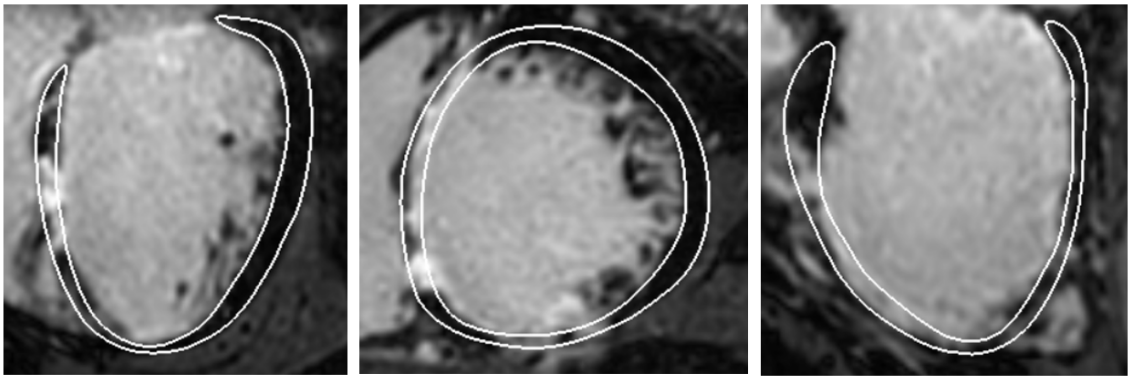

Figure 6: Left ventricle endocardial and epicardial delimitation of patient 2 in *Adas3D*. *Left image:* Sagittal plane. *Middle image:* Transversal plane. *Right image:* Coronal plane.

The 3D ventricular model was divided into 10 layers from the endocardium to the epicardium, each layer representing 10% of the total LV wall thickness, obtaining a 3D shell for each layer. Then, in order to have a myocardial scar characterization, a pixel signal intensity-based algorithm is applied in the software. The three tissue types (BZ, CZ and healthy tissue) were differentiated using thresholds of 60±5% and 40±5% of the maximum pixel intensity signal. The algorithm classifies the tissue as CZ if pixel values are above 60±5%, as BZ if pixel values are comprised between 40±5% and 60±5%, and as healthy tissue if pixel values are below 40±5%. Depending on the resolution of the CMRs, these thresholds can be modified. However, for the 15 cases segmented in this project, the previously mentioned thresholds were used. Figure 7 shows the final LV segmentation of one of the analyzed cases.

Moreover, *Adas3D* allows to automatically detect border zone channels (BZC), which consist on continuous corridors of BZ surrounded by scar tissue or an anatomical barrier connecting two areas of healthy tissue. These BZCs could correspond to the alternative CCs causing the reentry circuits to appear. Once tissue differentiation and BZC were obtained, quantitative results could be extracted from *Adas3D*, with the aim of making a comparison between patients.

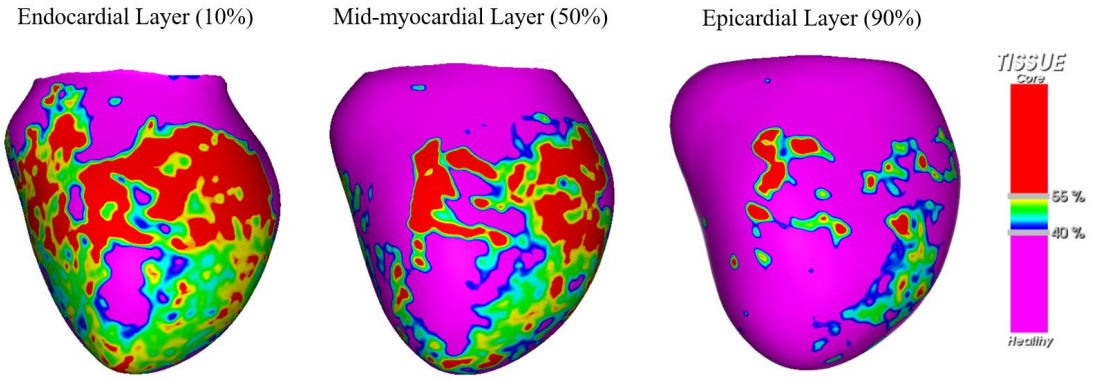

Figure 7: Three-dimensional left ventricle segmentation of patient 2 in *Adas3D*. Septal-anterior view of the infarct scar in endo-, mid- and epicardial layers. A threshold of 55% for core zone and 40% of healthy tissue was used. Red area: Core zone; Blue-Green-Yellow area: Border one; Purple area: Healthy tissue.

After obtaining the necessary information of the LV, the RV was also segmented in order to further perform the simulations in biventricular models. The pipeline followed was the same as for the LV, however, in the RV no tissue characterization was needed. For this purpose, only the RV anatomy was segmented, as shown in Figure 8, where the 15 biventricular models can be observed.

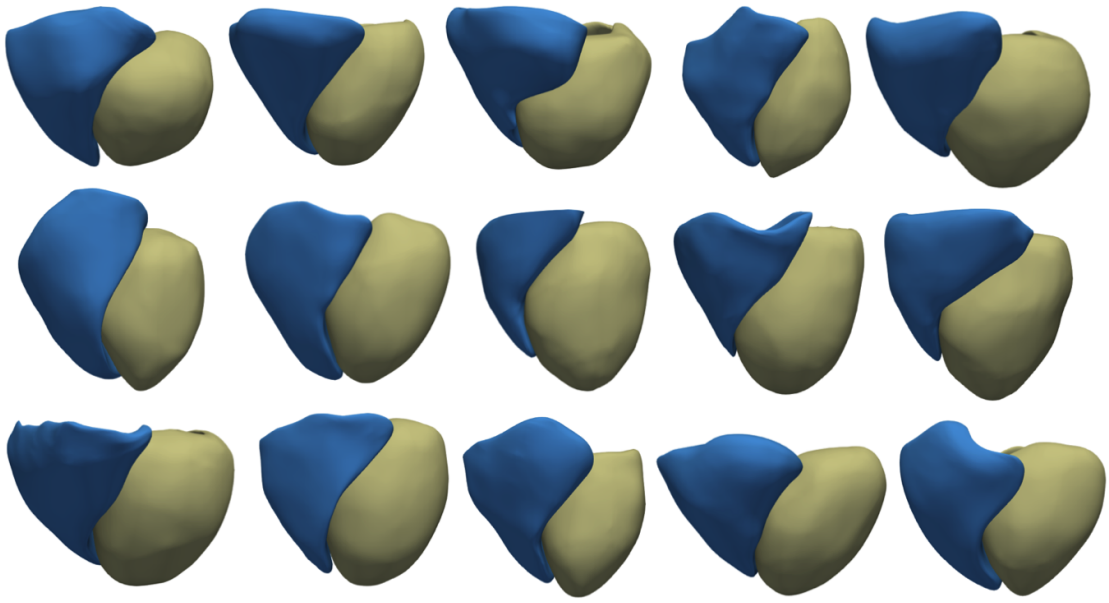

Figure 8: Three-dimensional right and left ventricles segmentations of the fifteen patients in *Adas3D*. Left ventricle: yellow anatomy. Right ventricle: blue anatomy.

2.3 Patient-specific model reconstruction in the cellular automata

Once the LV image was obtained and the model was processed and correctly labelled with *Adas3D*, a geometrical mesh was obtained. From here, different steps needed to be carried out in order to build the computational model in the CA.

2.3.1 Left ventricle geometrical model

Since *Arritmic3D* is an automata-based tool, there was no need to generate a surface and a volumetric mesh. Instead, the model obtained from *Adas3D* needed to be discretized in order to carry out the simulations in the CA. *Arritmic3D* includes a pre-processing tool that is able to build automatically the discretized computational model.

First, from the segmented *Adas3D* model, 5 meshes were obtained: a CZ, a BZ, an endocardium, an epicardium and a geometrical mesh of the LV, as can be observed in Figure 9. Once these 5 meshes were obtained, the first part of this pre-processing tool consisted of voxelising these files. To do this, all the data was loaded into a Python file, made apart from the CA simulator. In order to correctly voxelize the models, it was very important that the resolution of the CMR was within a valid margin, otherwise the discretization could not be done.

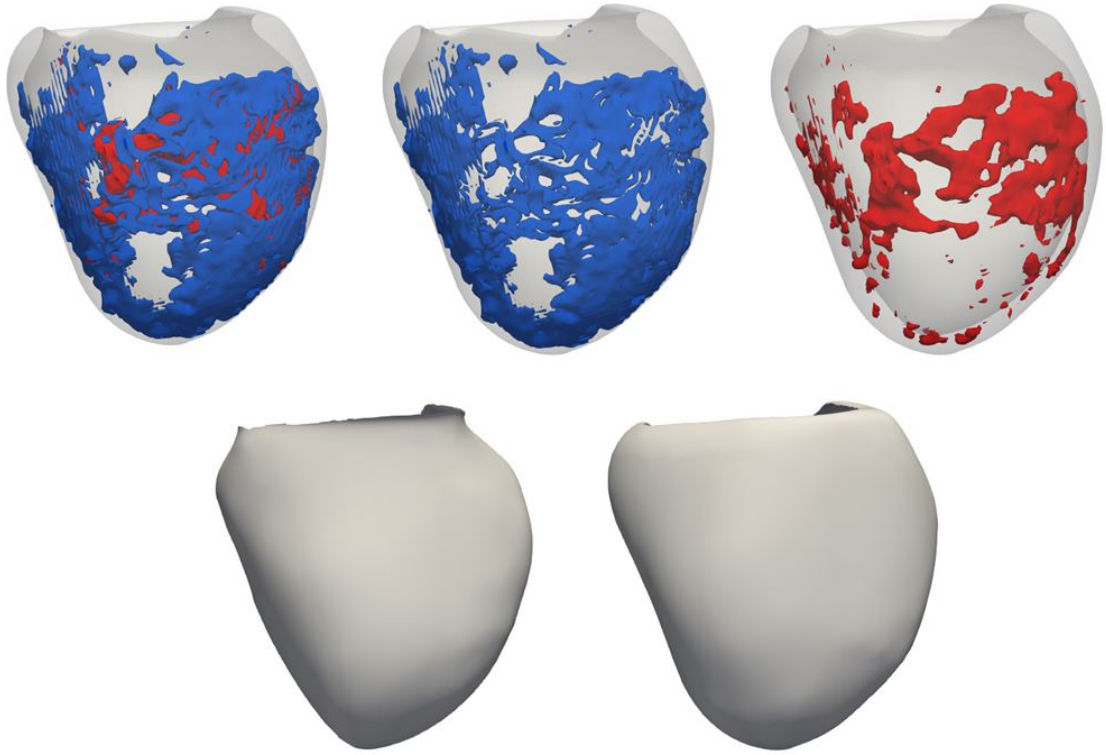

Figure 9: 3D meshes of patient 2 obtained from *Adas3D*. The first row corresponds to the left ventricle geometrical mesh with the border zone and core zone, represented in blue and red, respectively. The second row represents the endocardium mesh (left) and the epicardium mesh (right).

By means of implicit functions, the limits of the ventricular model were determined and the number of cells belonging to it was evaluated, obtaining the geometry of the ventricle. As the information obtained was in scalar values, the data was converted to points, extracting the geometry of the voxelised ventricle. From here, different arrays were created where different types of information were stored: (i) 3 arrays to define the coordinates of the nodes of each cell (x,y,z); (ii) 3 arrays to define the fiber orientation in the different directions (x,y,z); (iii) 1 array to store the intensity values of each cell. Then, different implicit functions evaluated the cells belonging to each mesh type (CZ, BZ, epicardium, endocardium), and subsequently, different arrays stored the value of each cell type.

Next, to determine the fiber orientation, the Streeter's method [47] was used. First, the vector of the longitudinal axis of the ventricle was calculated, between the point defined as the apex and the centroid of the base, which would correspond to the location of the mitral valve. Then, the vector normal to the endocardium and epicardium was calculated for each node. To define the fiber orientation vector, two angles are defined: *helix angle*, which takes into account the distance from the endocardium to the epicardium, and the *transmural angle*, which takes into account the distance from the apex to the base. The obtained fibre orientation vector must then be converted from global to local coordinates. Once converted to local coordinates, the direction of the cardiac fibre orientation was defined in separate coordinates (x,y,z), as these coordinates would later be inputs for when the simulations were loaded. With the parameters defined, the model was created as a set of simplified 3D slabs of tissue with regular hexahedral elements of 0.3 mm. As a result, a file containing the voxelised model with all the case data included was obtained, as it can be shown in Figure 10.

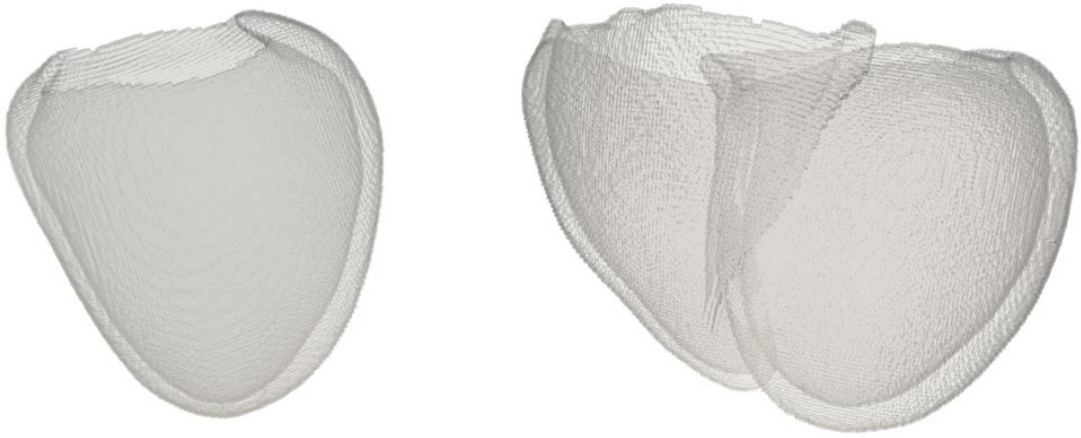

Figure 10: Voxelized left ventricle *(left)* and biventricular model *(right)* of patient 2, after preprocessing tool in *Arritmic3D* performs the discretization of the model obtained in *Adas3D*.

2.3.2 Electrophysiological model

The CA implemented in *Arritmic3D* mimics the behaviour of a biophysical model, with the advantage of performing the simulations with a very low computational cost. The model was defined as a 4-tuple, an ordered set of objects characterised by the following components: CA = (L,S,V,θ). First, each cell of the model included the integer lattice, L, which is defined by four parameters:

(i) The geometrical location.
(ii) The cell type (endocardial, mid-myocardial and epicardial).
(iii) The cell status (healthy tissue, BZ and CZ).
(iv) The cell threshold to move from resting to activated state.

Fiber orientation and tissue connectivity are encoded in the conduction velocity (CV), which is specific to each CA node. Then, S corresponds to the finite set of all possible cell states, which are three: *inactivated* or *repolarized*, when the cell remains relaxed and excitable, *activated* or *depolarized*, when the cell is able to activate neighbours, and *refractory*, when the cell is activated but it is not able to activate neighbours. V is the finite set of cells that define the neighbourhood for a cell, and θ is a transition function applied simultaneously to the cells that make up the lattice. To simulate electrophysiology in the model, each element in the CA is represented as a node, representing a portion of cardiac tissue, and not a single cardiac cell. The electrical propagation of cardiac tissue occurs as follows: when a repolarized node gets excited, it activates itself and the surrounding nodes. This node remains active during its action potential duration (APD), and does not allow further activation until its APD has finished. Once it expires, the node repolarizes again. Besides, when a node is depolarized, the activation of the neighbours does not occur immediately, it depends on the CV and the distance between the deactivation and the next activation of the nodes, known as diastolic interval (DI).

Furthermore, to make the electrophysiological model more precise, additional properties were also included. One was the APD memory, which ensured smooth changes in the APD in response to large cycle gradients (i.e., when pacing protocols are applied). Electrotonic coupling effects were also considered, especially in those regions where different type of cells were in contact. For this project, an APD memory of 0.05 and an electrotonic coupling effect of 0.6 were applied for all patients. Furthermore, a cardiac safety factor (CSF) was implemented, which is a measure that describes the robustness of propagation in cardiac tissue.

2.4 Clinical pacing protocol

In the clinical setting, EPS are decisive in determining whether a patient might suffer from arrhythmias. Different pacing protocols can be applied, depending of the type of arrhythmia to be detected. For patients who have suffered a MI, arrhythmia inducibility by ventricular pacing during an EPS is crucial to test the functionality of scar-related circuits, to find out whether alternative CCs actually cause VTs. Nonetheless, the pacing protocols defined to induce VTs are slightly different between hospitals.

For this project, the actual clinical pacing protocol applied at *Centro Médico Teknon* when testing VT inducibility in post-MI patients was followed. For the pacing to be carried out, a tetrapolar catheter is first introduced through the right femoral artery and guided to the right atrium. Then, the catheter goes through the tricuspid valve and enters the RV. Once inside the RV, the catheter is placed at the apex, and there they try to induce a VT. Therefore, since the RV endocardium is being excited first, electrical activation will reach the LV through the septal wall, from the epicardium to the endocardium.

The main objective was to virtually pace from the RV apex, however, in the case where no RV was considered, as in the first setup, more pacing sites were defined. In order to decide which other pacing locations would be the most optimal, experienced electrophysiologists at *Centro Médico Teknon* suggested the the most common pacing sites: the RV and LV septal walls. For the first setup, in which only the left ventricular model was considered, pacing was implemented from the LV apical and mid-epicardium, since it was the closest location to the RV apex. For this purpose, two pacing locations were defined at the LV epicardium, as shown in Figure 11:

1) Apical Epicardium (LV Apical-Epi)
2) Mid Epicardium (LV Mid-Epi)

Moreover, in order to analyze more pacing locations, endocardial pacing sites were also defined. As the electrophysiologists suggested pacing from the septal wall, three pacing sites at the LV endocardium were defined, as observed in Figure 11:

3) Basal Endocardium (LV Basal-Endo)
4) Mid Endocardium (LV Mid-Endo)
5) Apical Endocardium (LV Apical- Endo)

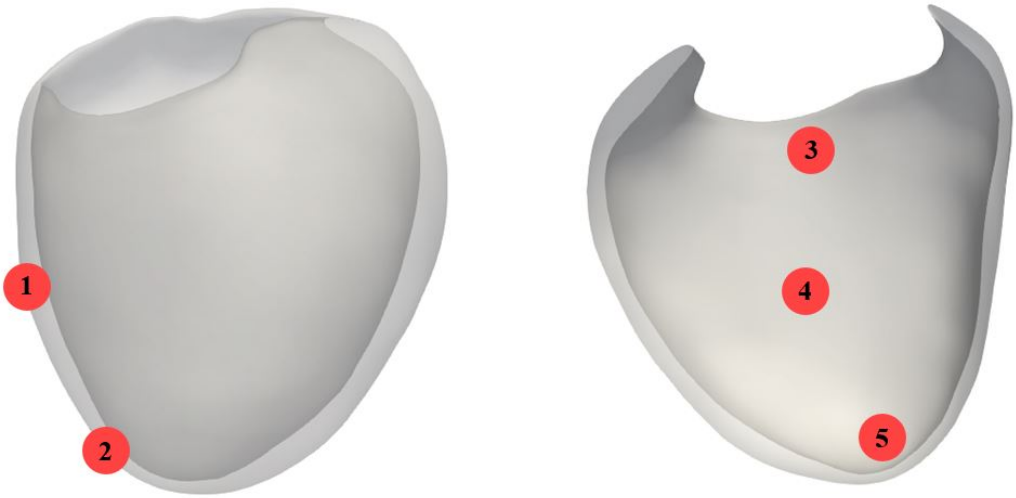

Figure 11: Pacing sites determined for LV. *Left image*: epicardial pacing sites. *Right image*: endocardial pacing sites.

As mentioned above, a biventricular model was also generated. The model was composed of the two ventricles separately, being the septal wall the only region of union between both. For this biventricular model, two RV pacing sites were defined, recreating the actual pacing performed in the EPS, as shown in Figure 12. The pacing sites considered were:

6) Apical Endocardium (RV Apical-Endo)
7) Mid Endocardium (RV Mid-Endo)

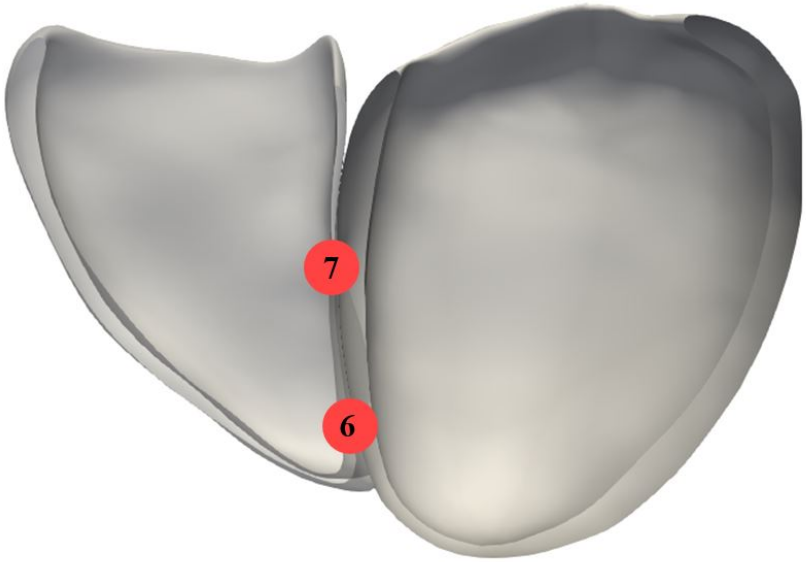

Figure 12: Pacing sites determined for RV.

For each patient and for each pacing site, an ID point was selected in *Paraview* (Kitware Inc. and LANL, NY, USA) by manually selecting a node located in the region of interest. Then, the ID of the different pacing sites was introduced into the corresponding input file to run the *Arritmic3D* simulations. After deciding the pacing locations, the clinical pacing protocol showed in Figure 13 was virtually applied:

(i) A base cycle (S1), which consisted of applying a train of 8 stimuli with a cycle length (CL) of 430 ms, was defined.

(ii) An extra stimulus (S2) with an initial CL of 300 ms was added. If no VT was induced, the CL of S2 decreased in steps of 10 ms until the refractory period was reached or until S2 had a CL of 200 ms.

(iii) S2 was increased 20 ms and a second extra stimulus (S3) with the same CL of S2 was added. The same protocol as for S2 was followed with S3, and if no VT was induced, a final extra stimulus (S4) was applied.

(iv) If S4 also failed to induce VT, the CL of S2 and S3 was decreased in steps of 10 ms until all three extra stimuli reached a CL of 200 ms, if they did not reach refractory period before.

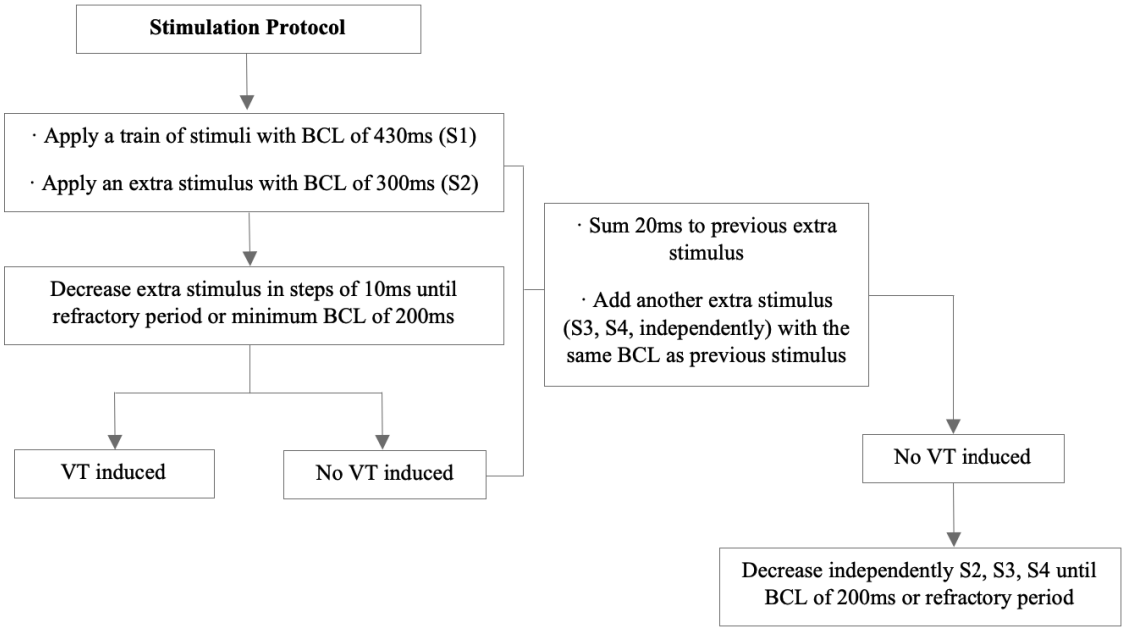

Figure 13: Diagram of the pacing protocol applied based on the one implemented in *Centro Médico Teknon*.

After performing the simulations with the described pacing protocol, the results obtained could be three: sustained ventricular tachycardia (SVT), non-sustained ventricular tachycardia (NSVT) or no ventricular tachycardia (No VT).

In a real EPS, if we ended up having the three extra stimuli (S2, S3, S4) with a minimum coupling of 200 ms and there was no VT induced, the study would be repeated under infusion of *Isoproterenol*, a drug that increases the induction of arrhythmias by increasing the baseline heart rate. If by repeating the EPS under *Isoproterenol* effects no VT is induced, that means that the patient is not at risk of suffering VT episodes. Nevertheless, if during the pacing protocol some VT was induced, that implies that the patient is at a high risk of developing future arrhythmic events.

2.5 Simulation setup

Arritmic3D is a novel CA-based software created specifically to simulate the dynamic properties of human myocardium in healthy and post-infarct conditions, in order to efficiently simulate the electrical activity in patients who have suffered a MI with low computational cost. This simulator has been developed by the CoMMLab research group led by Pr. Rafael Sebastian at *Universitat de València*.

Before starting with the simulations, different initial parameters had to be defined. The *Arritmic3D* software has 2 main folders after installation: "*Readers*", which contains the Phython code that generates the voxelized models from the meshes obtained in the segmentation, and "*arritmic3D*", where the main files that generate the simulations are located.

Within the *arritmic3D* folder, 3 files are needed as input for the simulations to work:
- **cases**: a general folder where sub-folders for each patient have to be created. Inside each patient's folder, there will be a folder called "*Readers_ VTK*" with all the data of the voxelized model and a file named "*params.dat*", in which all the case parameters can be modified.
- **restitutionCurves**: a folder corresponding to the restitution curves of APD and CV for the different cell types (CZ, BZ, healthy) in the different layers (endo, mid, epi).
- **paramsInit.dat**: a file that allows to modify the number case option and the case folder name the user wants to simulate.

The rest of the files found in the *arritmic3D* folder are general for all ventricular geometries. Once the input files are correctly defined, the file *arritmic3D.psc* is used to perform the simulations. For the simulations carried out in this work, the average time taken for a 10,000 ms simulation was of 10 minutes per patient.

2.6 Validation metrics

To validate in-silico simulations, the measurements obtained from patients in the EPS were acquired to compare whether they matched those obtained in the simulations. In addition, scar characteristics were extracted from *Adas3D* with the aim of making a comparison between patients and provide information on the arrhythmogeneity of the scar. The scar values used were the following:

- Scar, BZ, CZ mass with respect to the total LV mass (g).
- Scar percentage with respect to the total LV mass (%).
- BZ and CZ percentage with respect to the total scar mass (%).
- BZC mass (g).

Finally, for visual validation of reentry circuits, BZCs detected in *Adas3D* were used, since they could be useful to visualize possible reentry circuits during the LV activation propagation after pacing.

3 Results

This section includes the results obtained from the simulations of patient-specific 3D cardiac models. Fifteen patients with previous MI were evaluated with the aim of predicting whether they would have VTs induced. The results obtained were compared with the real results each patient obtained during an EPS. A total of 105 simulations were performed to validate with real data.

3.1 Clinical data and scar characterization

The clinical and scar characteristics were analysed in Table 1 as a function on whether patients had VT induced during an EPS or not. Difference in scar mass was noticeable between patients with and without induced VT (43.9 ± 31.2 vs. 15.6 ± 7.3) and the opposite pattern was observed in LVEF (32.5 ± 4.5 vs. 52.0 ± 8.8). In general, a high scar mass and a low LVEF was observed in patients with induced VT during EPS, and the opposite behaviour was observed with non-induced VT patients; a lower scar mass and a higher LVEF. The two patients without an EPS presented a higher scar mass than patients with non-induced VT but a lower mass than those with induced VT.

In addition, the BZ and CZ masses varied according to the scar mass value, being the BZ mass always higher than the CZ mass. It could also be seen that the mean age was similar in the three groups of patients, while there was a great disproportion in terms of the sex of the patients, as only one of the fifteen was female.

	Total	Induced VT	No Induced VT	No EPS
N	15	7	6	2
Clinical characteristics				
Female sex	1	0	1	0
Male sex	14	7	5	2
Age (years)	65.4 ± 10.6	66.5 ± 13.2	65.8 ± 7.3	60.0 ± 14.1
LVEF (%)	42.8 ± 11.7	32.5 ± 4.5	52.0 ± 8.8	51.0 ± 5.6
Scar characterization				
Scar mass (g)	29.5 ± 25.9	43.9 ± 31.2	15.6 ± 7.3	20.8 ± 22.6
BZ mass (g)	20.6 ± 16.5	30.6 ± 8.7	11.2 ± 5.7	13.8 ± 14.7
CZ mass (g)	8.9 ± 10.4	13.3 ± 13.7	4.3 ± 2.9	6.9 ± 7.9

Table 1: Mean ± standard deviation of the clinical and scar characteristics of the fifteen patients.

3.2 Ventricular tachycardia induction

All fifteen cardiac models were virtually stimulated following the in-silico pacing protocol described in Section 2.4. The simulations results of the seven patients with induced VT during EPS can be observed in Table 2. RV and LV main columns are in-silico results obtained for each of the pacing sites described. Right column shows the results each patient obtained during the EPS. Focusing on LV pacing, overall, epicardial pacing had a higher rate of success than endocardial pacing. Both epicardial pacing sites (*mid* and *apical*) obtained similar results, except from patients 6 and 12, which obtained the opposite results. Nevertheless, in comparison with the actual results obtained during EPS, in epicardial LV pacing, 5 of the 7 patients achieved the same results. Conversely, endocardial pacing of the LV had a lower success rate. Only in patients 1, 3, 4 and 5 a SVT event was correctly detected in at least one of the three different pacing sites, being apical pacing the less robust.

On the other hand, in RV pacing, apical-endocardial pacing achieved better results than mid-endocardial pacing, being the results obtained in the apical zone almost equal to the real data. However, for patient 6 no VT event was detected in any of the two pacing locations.

	RV		LV					EPS
	Mid-Endo	Apical-Endo	Mid-Epi	Apical-Epi	Basal-Endo	Mid-Endo	Apical-Endo	RV Apical-Endo
P1	NO VT	**SVT**	**SVT**	**SVT**	**SVT**	**SVT**	NO VT	SVT
P2	NO VT	**SVT**	**SVT**	**SVT**	NSVT	NO VT	NO VT	SVT
P3	**SVT**	**SVT**	**SVT**	**SVT**	**SVT**	NO VT	NO VT	SVT
P4	**SVT**	**SVT**	NO VT	NO VT	NO VT	NO VT	**SVT**	SVT
P5	**SVT**	**SVT**	**SVT**	**SVT**	NO VT	**SVT**	NO VT	SVT
P6	NO VT	NO VT	**SVT**	NO VT	NO VT	NO VT	NO VT	SVT
P12	**SVT**	**SVT**	NO VT	**SVT**	NO VT	NO VT	NO VT	NSVT

Table 2: Results of in-silico pacing sites of patients with induced VT during EPS compared to real clinical outcomes. Bold results correspond to correct outcomes matching with EPS. SVT: Sustained Ventricular Tachycardia, NSVT: Non-Sustained Ventricular Tachycardia.

Each patients' probability of having an induced virtual VT was calculated based on the correct events detected by the different pacing sites, as shown in Table 3. In patients 1-3 and 5 the probability of having an induced VT event exceeded 50%. On the contrary, patients 4, 6 and 12 obtained a probability of less than 43%. In patient 4, a SVT was detected only in three of the seven pacing locations (*RV-Apical-Endo* and *LV-Apical-Endo*), as well as in patient 12 (*RV-Apical-Endo* and *LV-Apical-Epi*), whereas only a single SVT event was detected in patient 6 (*LV-Mid-Epi*). Moreover, RV and LV pacing sites were unable to detect the NSVT of patient 12.

	P1	P2	P3	P4	P5	P6	P12
VT (%)	71.4	50.0	71.4	42.8	71.4	14.2	42.8

Table 3: Patients' probability of having induced VTs based on in-silico results. Selected patients had a positive outcome during the EPS.

Table 4 shows the results for patients who did not have induced VT during EPS. LV endocardial and epicardial pacing obtained similar results, since for every of the five pacing sites, at least in one patient a SVT event was detected. For RV pacing, the apical pacing site obtained the same results as the real data, while in the mid pacing site only one patient was detected with a SVT. The same results were achieved in patients 7, 11 and 13, while at least two SVT events were detected in patients 9, 14 and 15. Patients 9 and 15 obtained a SVT in two pacing locations (*LV-Basal-Endo* and *LV-Apical-Endo* in patient 9 and *RV-Mid-Endo* and *LV-Apical-Epi* in patient 15). Patient 14 obtained the poorest results, with a SVT event detected in three pacing locations, all from the LV (*Mid and Apical-Epi* and *Mid-Endo*). Nonetheless, the probability of having a VT induced in these three patients did not exceed 43%, as shown in Table 6.

	RV		LV					EPS
	Mid-Endo	Apical-Endo	Mid-Epi	Apical-Epi	Basal-Endo	Mid-Endo	Apical-Endo	RV Apical-Endo
P7	**NO VT**	**NO VT**	**NO VT**	**NO VT**	**NO VT**	**NO VT**	**NO VT**	NO VT
P9	**NO VT**	**NO VT**	**NO VT**	**NO VT**	SVT	**NO VT**	SVT	NO VT
P11	**NO VT**	**NO VT**	**NO VT**	**NO VT**	**NO VT**	**NO VT**	**NO VT**	NO VT
P13	**NO VT**	**NO VT**	**NO VT**	**NO VT**	**NO VT**	**NO VT**	**NO VT**	NO VT
P14	**NO VT**	**NO VT**	SVT	SVT	**NO VT**	SVT	**NO VT**	NO VT
P15	SVT	**NO VT**	**NO VT**	SVT	**NO VT**	**NO VT**	**NO VT**	NO VT

Table 4: Results of in-silico pacing sites of patients with not induced VT during EPS compared to real clinical outcomes. Bold results correspond to correct outcomes matching with EPS. SVT: Sustained Ventricular Tachycardia, NSVT: Non-Sustained Ventricular Tachycardia.

An analysis was also performed on the two patients who did not undergo an EPS, although no comparison with real data could be made. In Table 5, and looking at the results of Table 6, a clear difference between the results of both patients could be observed. For patient 8 the probability of having an induced virtual VT was of 0%, while for patient 10 it was of 57.1%, with SVT events being detected in four pacing sites (*RV endo* and *LV epi*).

	RV		LV					EPS
	Mid-Endo	Apical-Endo	Mid-Epi	Apical-Epi	Basal-Endo	Mid-Endo	Apical-Endo	RV Apical-Endo
P8	NO VT	NO VT	NO VT	NO VT	NO VT	NO VT	NO VT	NP
P10	SVT	SVT	SVT	SVT	NO VT	NO VT	NO VT	NP

Table 5: Results of in-silico pacing sites of patients without EPS. SVT: Sustained Ventricular Tachycardia, NSVT: Non-Sustained Ventricular Tachycardia, NP: Not Performed.

	P7	P8	P9	P10	P11	P13	P14	P15
VT (%)	0	0	28.5	57.1	0	0	42.8	28.5

Table 6: Patients' probability of having induced VTs based on in-silico results. Patients 7, 9 and 11-13 had a negative outcome during the EPS, while patients 8 and 10 did not undergo an EPS.

Table 7 shows the percentage accuracy of each pacing location. To calculate the accuracy values, the two patients who did not undergo EPS were excluded. The locations with the highest percentage of accuracy were both RV pacing locations and the two LV epicardial locations, with apical RV pacing having the highest accuracy (92.3%). On the other hand, LV endocardial pacing presented lower values, being the apical endocardial location the one with the lowest percentage (46.1%).

Pacing sites	Accuracy (%)
RV Mid-Endo	69.2
RV Apical-Endo	92.3
LV Mid-Epi	76.9
LV Apical-Epi	69.2
LV Basal-Endo	53.8
LV Mid-Endo	53.8
LV Apical-Endo	46.1

Table 7: Accuracy of pacing sites.

The percentage of scar mass with respect to the LV mass is shown in Figure 14. Each scar percentage has an associated percentage of BZ and CZ, which varies in every patient. It can be noticed that patients 1, 3, 4, 10, 12 and 15 had a scar mass higher than 20%, while patients 8, 9 and 11 presented a scar mass below 10%, having a smaller scar. In general, patients with SVT induced on EPS presented a higher percentage of scar than those who did not have VTs induced. It can also be observed that there were patients with a similar percentage of BZ and CZ, such as patients 3, 4, 10 and 13, while in the rest of the patients the percentage of BZ was much higher than the CZ.

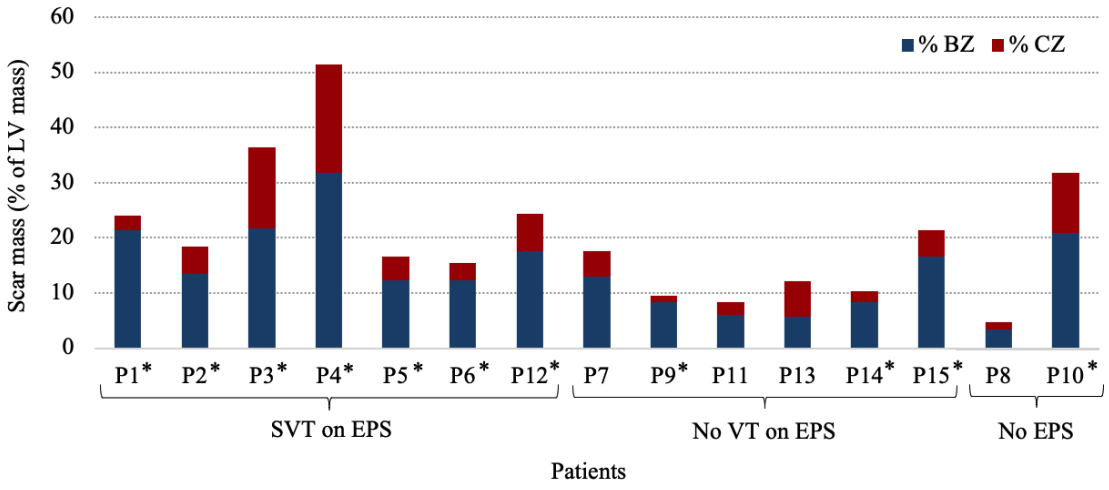

Figure 14: Scar mass heterogeneity. Patients with (*) had in-silico induced SVT in at least one pacing site. SVT: Sustained ventricular tachycardia.

Figure 15 shows the BZC mass of each patient obtained using *Adas3D*. Patients 1, 3, 4 and 15 had the highest channel mass, above 15 grams. Patients 2, 5, 6, 10 and 12 presented a channel mass below 15 grams but above 5 grams, while patients 7 and 14 had a mass below 4 grams, being not as significant. Finally, no channel mass was detected in patients 8, 9, 12 and 13. A noticeable difference in BZC mass between patients with and with no SVT detected on the EPS can be observed, being those with SVT the ones presenting a higher mass. Moreover, patients in which a SVT event was detected in-silico correspond to those that present BZC mass, except from patient 7.

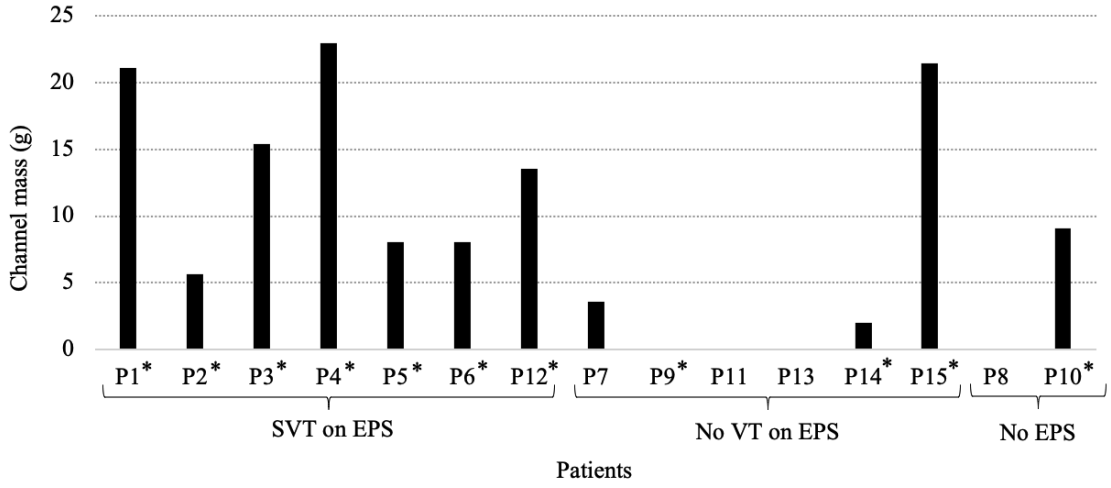

Figure 15: BZC mass. Patients with (*) had in-silico induced SVT in at least one pacing site. SVT: Sustained ventricular tachycardia, BZC: Border zone channel.

Regarding the visualization of the reentry circuits, Figure 16 shows the activation of the BZ region of one of the analyzed cases, where colors correspond to myocytes' life-time. After applying a S1-S4 protocol (S1: 430 ms | S2: 300 ms, S3: 280 ms, S4: 270 ms) at the RV apex (black dot), a reentry circuit was generated. A conduction block is observed 30 ms after S4 pacing (black cross). Then, the arrows show the direction of the wavefront, and almost 200 ms after S4 pacing, the slow CC can be seen. This slow channel caused by the last extra-stimulus corresponds to one of the BZCs detected in *Adas3D* (purple channel). In the end, it can be observed that the slow CC repolarizes the cardiac tissue, subsequently causing a SVT.

On the other hand, Figure 17 shows the BZ activation of myocytes after applying a S1-S3 protocol (S1: 430 ms | S2: 290 ms, S3: 260 ms) at the RV apical zone, at which a SVT was generated. After S3 pacing, a conduction block is observed (white cross) at the endocardial-septal wall. At 500 ms, the white arrows represent the region at which late activation was originated, although the reentry circuit generating it could not be detected. Then, 300 ms after pacing, a SVT is initiated.

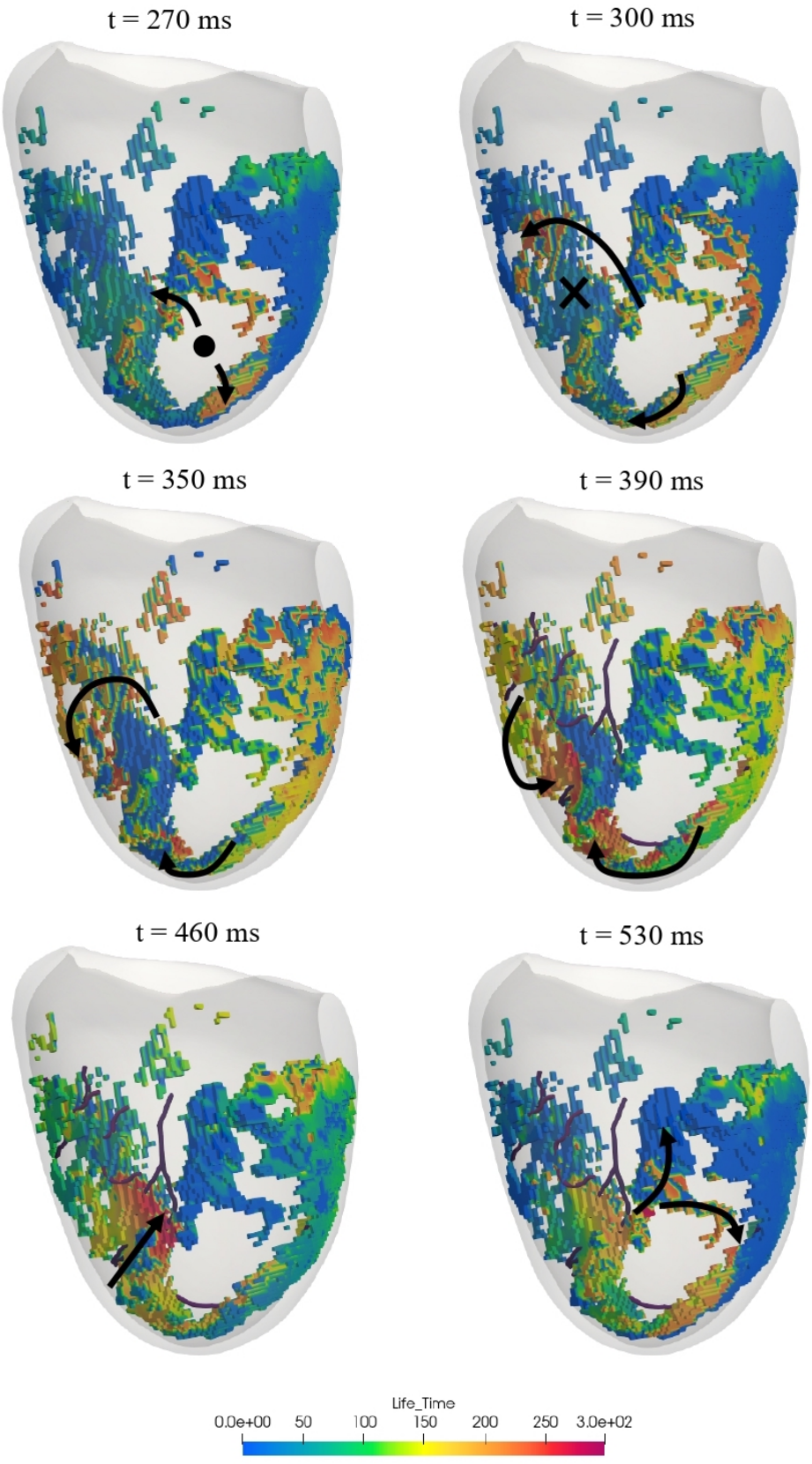

Figure 16: Simulation snapshots of patient 2 after applying a S1-S4 protocol (S1: 430 ms | S2: 300 ms, S3: 280 ms, S4: 270 ms) at the right ventricle apex (black dot). Colors correspond to the time to resting state. Purple tubes correspond to BZCs detected in *Adas3D*.

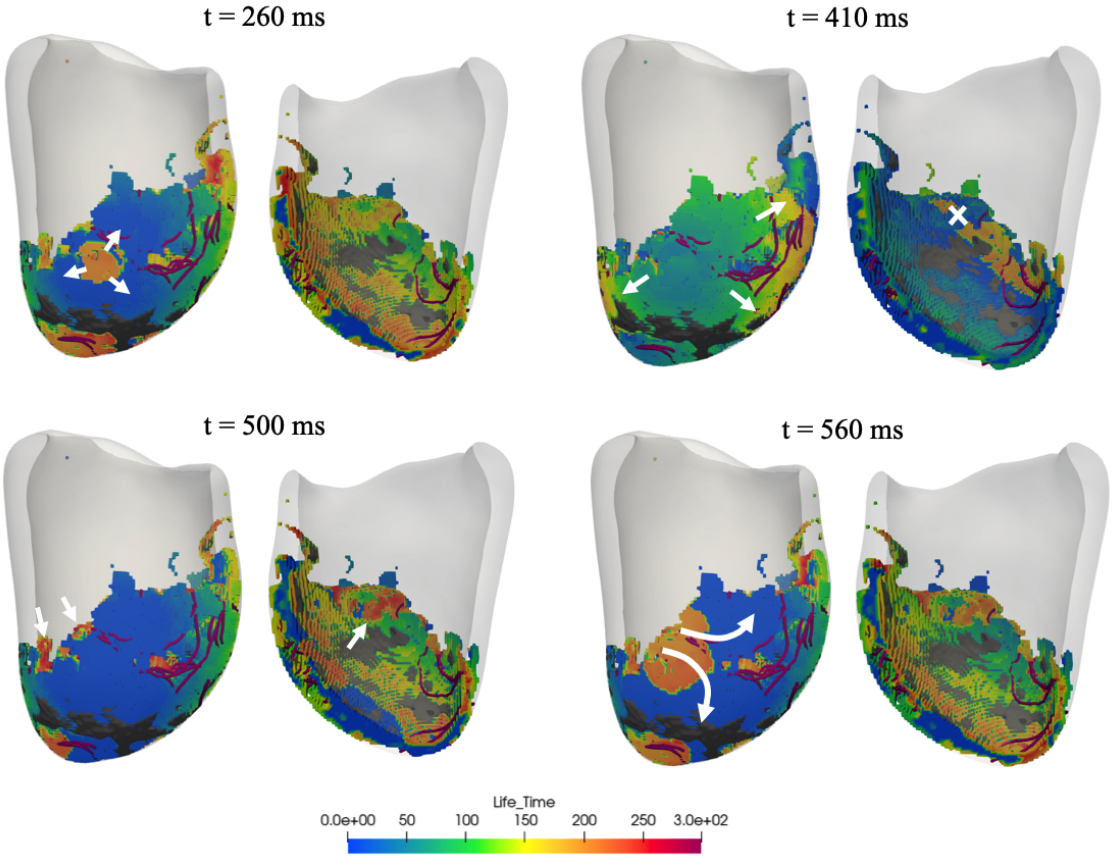

Figure 17: Simulation snapshots of patient 4 after applying a S1-S3 protocol (S1: 430 ms | S2: 290 ms, S3: 260 ms) at the right ventricle apical zone. Colors correspond to the time to resting state. Purple tubes correspond to BZCs detected in *Adas3D*. Left images show the epicardial-septal BZ wall of the left ventricle. Right images show the endocardial-septal BZ wall of the left ventricle. BZ: Border zone.

4 Discussion

The present project describes a pipeline to perform LV electrophysiological simulations in patients who have a heterogeneous scar due to MI, making it possible to stratify VT risk in these patients in a non-invasive way. Such study was carried out in 15 patients. A virtual pacing protocol simulating the real protocol used in the clinic was implemented, and fast electrophysiological simulations were performed with the aim of making the simulations as similar as possible to the pipeline followed in the clinical practice.

4.1 Simulations results

Results of the scar mass characterization showed correlation with the results of the BZC mass [32]. Patients with a scar mass that occupied more than the 20% of the total LV mass (see Figure 14) also presented a higher BZC mass (see Figure 15). This correlation could be observed in patients 1, 3, 4, 10, 12 and 15. Analysing the percentages of scar mass, those with a higher percentage of BZ than of CZ were the ones with more arrhythmogenic substrate. Regarding patients with induced VT during EPS, comparing the results of the simulations (see Table 2) with the scar metrics (see Figure 14), patients with a percentage of CZ inferior than the percentage of BZ presented a higher probability of virtually inducing VT and a greater amount of BZC, except patients 4, 6 and 12. Although patient 4 had the largest scar and BZC mass, the probability of VT detection was not very high, as it happened with patients 6 and 12. This may be due to the fact that myocyte propagation was not well detected in the voxelized models, because the alternative CC were small and more difficult to detect, or it could rely on the fact that the basal conditions of the patient were not considered. Despite these less accurate results, for each of the seven patients who had induced VT during the EPS, at least one in-silico pacing location detected a VT episode. This demonstrated that the models, although being less detailed, were able to reproduce VT re-entrant behaviour.

Regarding patients with non-induced VT at the EPS, patients in whom no VT event was virtually induced tended to be those with no or very low BZC mass. Nevertheless, in patient 9, although not having BZC, SVT was detected at two pacing sites. As stated above, perhaps the fact that the BZ was much higher than CZ is what led to the detection of alternative CCs during cell propagation, as it was the case of patient 14. Virtual simulations showed that patient 14 had a high probability of suffering a VT event despite of the low scar and BZC mass. On the contrary, patient 15 presented a very high BZC mass ($<$20%) and a probability of virtually inducing a VT of 28.5%, although in the EPS the result was negative. Such large discrepancy on this patient's results demanded experts' opinion. After sharing the results with electrophysiologists at *Centro Médico Teknon*, the conclusion reached was that perhaps when the patient underwent the EPS, the patient's baseline conditions at that time were such that no VT was induced. This idea was proposed since, based on the high BZC mass and the results obtained in the simulations, it made more sense to have induced VT than not to have it.

As for patients 8 and 10, since they did not undergo an EPS, the results could not be compared with real data. Patient 8 had a zero probability of inducing virtually a VT. The scar mass was very low (see Figure 14) and did not present BZC mass (see Figure 15), being reasonable with the simulation results obtained. In patient 10 the opposite behaviour was observed. If this patient had an EPS performed, the results showed in Table 5 and in Figures 14 and 15 suggested that the outcome would be positive, since a 57,1% probability of virtually inducing a VT was obtained. Also, it presented a large scar (<30%) and BZC mass.

With respect to the pacing sites, one of the objectives of this project was to simulate the pacing site at the same place in which is performed in clinical practice: at the RV apex. By analysing the accuracy of the seven pacing sites, the in-silico RV apical-endocardial pacing site achieved the best results (see Table 7), thus matching the results of clinical practice. On the other hand, the difference on accuracy between the epicardial and endocardial pacing sites at the LV took place because of the different conduction velocities of the epicardial and endocardial layers. The endocardium has a higher conduction velocity than the epicardium [46]. Based on this, the simulated conduction velocity in the endocardium might prevent the detection of slow CCs in the models, and thus re-entrant circuits. A slower conduction velocity of the epicardium could possibly have been the reason for the detection of alternative CCs that, with a higher conduction velocity, might not be detected.

Besides, although a LVEF<35% is the only primary prevention parameter considered in the approach to SCD, previous studies [33] stated that the scar mass is an independent predictor of adverse outcome, and could be a future parameter to consider for ICD placement in primary prevention of SCD. Table 8 at the Appendix showed that patients 2, 4, 6 and 12 had a LVEF $\leq$ 35%. These patients had a significative scar mass and presented VT events at the EPS and in the simulations (see Table 2), indicating that it may exist risk of SCD. These results demonstrated that the performance of LV patient-specific electrophysiological simulations, as previously reported in the work by Trayanova et al. [21], together with the characterization of the scar mass, could be a future non-clinical parameter, more accurate than the LVEF, to predict the risk of SCD associated with VT caused by post-infarction scar.

Lastly, the computational time required by the CA-based software to perform a 10.000 ms simulation was of 10 minutes. Therefore, although each patient obtained different results when applying the pacing protocol, the approximate total computational time required to complete the pacing protocol was of 35 minutes. Although the results do not yet correspond to the real times in clinical practice, this results contrasts with the simulation times that would be obtained with biophysical models, where a single 10.000 ms simulation would take more than 24 hours. Hence, fast simulations based on CA have demonstrated that are able to reproduce the electrophysiological properties of the LV with high reproducibility. This can be seen in the results, which are similar to those obtained during the EPS. This study confirms that fast simulations can be performed by progressively adapting to real pacing protocols duration while assessing arrhythmia propensity.

4.2 Limitations and further work

In the first case, the biventricular model needs to be improved. In the generated biventricular models, both ventricles were segmented independently, each with its epicardial and endocardial layers. However, for the model to be realistic, an epicardial layer should surround both ventricles to ensure proper propagation of cardiac cells. Due to the lack of this layer, there were some regions where the ventricles were not in contact with each other and, therefore, proper myocyte propagation could not be computed. On top of that, the RV segmentations need also be improved, since with DIXON sequences in the LGE-CMR it is difficult to visualize the RV anatomy, especially the basal and apical areas. For this reason, RV segmentations varied so much between patients, because the anatomy of the basal and apical zones could not be accurately distinguished. Although the simulation results obtained at the RV were quite accurate, it is necessary to improve the segmentations, perhaps by segmenting the RV from a CT image, to obtain more robust results.

Another aspect to highlight is the complexity of the visualization of reentry circuits during wavefront propagation. First, only the BZ region was computed for better visualization, as this region is where reentry circuits originate. However, the exported model showing the life-time propagation of the BZ nodes only allowed visualization of the external part of the BZ, not the activation that happened inside it (see Figure 16). Plus, based on the BZCs detected in the segmentation, most channels in the models were small and narrow, making it even more difficult to detect the re-entrant circuits causing the VT. In general, it was possible to identify in which region the reentry originated (see Figure 17), but not the exact circuit causing it. By correctly identifying the reentry circuits that originate the VT, a comparison with the BZCs detected in the segmentation can be done, to visualize if they correspond to the same slow conducting channels simulated, and helping in this way to optimize the VT-RFA procedure. Nevertheless, this comparison could only be done in one patient (see Figure 16), where indeed one of the BZC detected in the segmentation matched with the slow CC computed in-silico. In the rest of the patients where VT was induced, it was not possible to detect visually the reentry circuits. As possible further work, the division of 10 layers from the endocardium to the epicardium could help in the detection of reentry circuits, allowing a further analysis of each layer and the detection of the circuits originating the VT.

Finally, aside from the computational issues, another factor to be considered is the baseline condition of the patients. Although the exact baseline conditions of the patients during EPS were unknown, *Isoproterenol* was administered in some cases, improving the inducibility of the arrhythmia. The CA model could not take into account the effect of drugs, so it is possible that VT was not induced in some patients because drug administration was not contemplated. A possible next step to consider could be the incorporation of the effects that these drugs have on the physiology of patients, making it possible to identify cases in which VT was not inducible, but that under the effects of drugs could be detectable.

5 Conclusions

The current bachelor thesis aimed to present a pipeline for performing fast LV electrophysiological simulations able to stratify the risk of VT in patients that have suffered a MI by following the steps that are carried out in the clinical practice.

The similarity of the results obtained in-silico with those obtained in EPS demonstrate that CA-based fast cardiac electrophysiology simulators together with the implementation of the pacing protocols used in real interventions are valid for assessing arrhythmia risk. The virtual implementation of the same pacing protocols is clearly necessary to test and validate the behaviour of the models. With that, it has been proven that the best in-silico pacing site matches that of EPS, demonstrating how relevant it is to perform cardiac simulations following the steps used in clinic.

Therefore, it is a step towards creating robust VA prediction models, which reliability would eventually reach the point where it could be considered as reliable as procedures performed in clinical practice. In this way, invasive EPS could be prevented by establishing in-silico models as a reliable parameter to assess VT risk.

Hence, with the aim of creating more accurate models, an improvement of the biventricular model used to perform the simulations is needed, and a better visualization of the electrical propagation would help on the detection of reentry circuits that cause the VT. On top of that, given that fast simulations are computed, this would enable studies with a larger number of patients, obtaining in this way greater sets of results that would help to reach more reliable conclusions.

Bibliography

[1] P. Markwerth et al. "Sudden cardiac death". In: *International Journal of Legal Medicine* 135 (2021), pp. 483–495. DOI: https://doi.org/10.1007/s00414-020-02481-z.

[2] P. Sanders et al. "Epidemiology of Sudden Cardiac Death: Global and Regional Perspectives". In: *Heart, Lung and Circulation* 28 (2019), pp. 6–14. DOI: 10.1016/j.pcad.2008.06.003.

[3] S.G. Priori et al. "2015 ESC Guidelines for the management of patients with ventricular arrhythmias and the prevention of sudden cardiac death". In: *European Heart Journal* 36.41 (2015), pp. 2793–2867. DOI: 10.1093/eurheartj/ehv316.

[4] J. J. Wellens Hein et al. "Risk stratification for sudden cardiac death: current status and challenges for the future". In: *European Heart Journal* 35.25 (2014), pp. 1642–1651. DOI: 10.1093/eurheartj/ehu176.

[5] N. Srinivasan and R. Schilling. "Sudden Cardiac Death and Arrhythmias". In: *Arrhythmia and Electrophysiology Review* 7 (2 2018). DOI: 10.15420/aer.2018:15:2.

[6] D. Vélez-Rodriguez. "ECG". In: *Marban* (2020).

[7] T. Leiner. "Deep Learning for Detection of Myocardial Scar Tissue: Goodbye to Gadolinium?" In: *Radiology* 291.3 (2019), pp. 618–619. DOI: 10.1148/radiol.2019190783.

[8] J. Feger. "Myocardial scar tissue". In: *Radiopaedia.org* (2020). DOI: https://doi.org/10.53347/rID-79486.

[9] F. Antoon et al. "Development of the Cardiac Conduction System". In: *Circulation Research* 82.6 (1998), pp. 629–644. DOI: 10.1161/01.RES.82.6.629.

[10] S. Sattler et al. "Ventricular Arrhythmias in First Acute Myocardial Infarction: Epidemiology, Mechanisms, and Interventions in Large Animal Models". In: *Frontiers in Cardiovascular Medicine* 6 (2019). DOI: 10.3389/fcvm.2019.00158.

[11] A. Goyal et al. "Reentry Arrhythmia". In: *StatPearls* (2022). URL: https://www.ncbi.nlm.nih.gov/books/NBK537089/.

[12] G. Larraitz et al. "Mecanismos de las arritmias cardiacas". In: *Revista Española de Cardiología* 65.2 (2012), pp. 174–185. DOI: https://doi.org/10.1016/j.recesp.2011.09.018.

[13] J. M. de Bakker et al. "Slow conduction in the infarcted human heart. 'Zigzag' course of activation." In: *Circulation* 88.3 (1993), pp. 915–926. DOI: 10.1161/01.CIR.88.3.915.

[14] S. L. Rutherford et al. "High-Resolution 3-Dimensional Reconstruction of the Infarct Border Zone". In: *Circulation Research* 111.3 (2012), pp. 301–311. DOI: 10.1161/CIRCRESAHA.111.260943.

[15] B. Jauregui et al. "Follow-Up After Myocardial Infarction to Explore the Stability of Arrhythmogenic Substrate: The Footprint Study". In: *JACC: Clinical Electrophysiology* 6.2 (2020), pp. 207–218. DOI: https://doi.org/10.1016/j.jacep.2019.10.002.

[16] A. Berruezo et al. "Three-Dimensional Architecture of Scar and Conducting Channels Based on High Resolution ce-CMR". In: *Circulation: Arrhythmia and Electrophysiology* 6.3 (2013), pp. 528–537. DOI: 10.1161/CIRCEP.113.000264.

[17] A. J. Moss et al. "Prophylactic Implantation of a Defibrillator in Patients with Myocardial Infarction and Reduced Ejection Fraction". In: *New England Journal of Medicine* 346.12 (2002), pp. 877–883. DOI: 10.1056/NEJMoa013474.

[18] J. E. Poole et al. "Prognostic Importance of Defibrillator Shocks in Patients with Heart Failure". In: *New England Journal of Medicine* 359.10 (2008), pp. 1009–1017. DOI: 10.1056/NEJMoa071098.

[19] D. Soto-Iglesias et al. "Cardiac Magnetic Resonance-Guided Ventricular Tachycardia Substrate Ablation". In: *JACC: Clinical Electrophysiology* 6.4 (2020), pp. 436–447. DOI: https://doi.org/10.1016/j.jacep.2019.11.004.

[20] S. H. Majeed et al. "Electrophysiologic Study Indications And Evaluation". In: *StatPearls* (2022). URL: https://www.ncbi.nlm.nih.gov/books/NBK567719/.

[21] D. Bahkta and JM. Miller. "Principles of electroanatomic mapping". In: *Indian Pacing Electrophysiology* 8.1 (2008), pp. 32–50. URL: PMCID:%20PMC2231602.

[22] A. Schmidt et al. "Infarct Tissue Heterogeneity by Magnetic Resonance Imaging Identifies Enhanced Cardiac Arrhythmia Susceptibility in Patients With Left Ventricular Dysfunction". In: *Circulation* 115.15 (2007), pp. 2006–2014. DOI: 10.1161/CIRCULATIONAHA.106.653568.

[23] J. C. Rubenstein et al. "A comparison of cardiac magnetic resonance imaging peri-infarct border zone quantification strategies for the prediction of ventricular tachyarrhythmia inducibility". In: *Cardiology Journal* 20.1 (2013), pp. 68–77. DOI: 10.5603/CJ.2013.0011.

[24] M. Disertori et al. "Myocardial Fibrosis Assessment by LGE is a Powerful Predictor of Ventricular Tachyarrhythmias in Ischemic and Nonischemic LV Dysfunction: A Meta-Analysis". In: *JACC: Cardiovascular Imaging* 9.9 (2016), pp. 1046–1055. DOI: https://doi.org/10.1016/j.jcmg.2016.01.033.

[25] R. D. Sebastiaan et al. "CMR–Based Identification of Critical Isthmus Sites of Ischemic and Non-ischemic Ventricular Tachycardia". In: *JACC: Cardiovascular Imaging* 7.8 (2014), pp. 774–784. DOI: https://doi.org/10.1016/j.jcmg.2014.03.013.

[26] B. Jáuregui et al. "Arrhythmogenic substrate detection in chronic ischaemic patients undergoing ventricular tachycardia ablation using multidetector cardiac computed tomography: compared evaluation with cardiac magnetic resonance". In: *EP Europace* 23.1 (2020), pp. 82–90. DOI: 10.1093/europace/euaa237.

[27] D. Andreu et al. "Cardiac magnetic resonance–aided scar dechanneling: Influence on acute and long-term outcomes". In: *Heart Rhythm* 14.8 (2017), pp. 1121–1128. DOI: https://doi.org/10.1016/j.hrthm.2017.05.018.

[28] A. Lopez-Perez et al. "Personalized Cardiac Computational Models: From Clinical Data to Simulation of Infarct-Related Ventricular Tachycardia". In: *Frontiers in Physiology* 10 (2019). DOI: 10.3389/fphys.2019.00580.

[29] NA. Trayanova et al. "Imaging-Based Simulations for Predicting Sudden Death and Guiding Ventricular Tachycardia Ablation". In: *Circulation: Arrhythmia and Electrophysiology* 10.7 (2017), e004743. DOI: 10.1161/CIRCEP.117.004743.

[30] J. Corral-Acero et al. "The 'Digital Twin' to enable the vision of precision cardiology". In: *European Heart Journal* 41.48 (2020), pp. 4556–4564. DOI: 10.1093/eurheartj/ehaa159.

[31] H. Arevalo et al. "Arrhythmia risk stratification of patients after myocardial infarction using personalized heart models". In: *Nat Commun* 7 (2016), p. 11437. DOI: https://doi.org/10.1038/ncomms11437.

[32] P. Sánchez-Sodomonte et al. "Scar channels in cardiac magnetic resonance to predict appropriate therapies in primary prevention". In: *Heart Rhythm* 18.8 (2021), pp. 1336–1343. DOI: https://doi.org/10.1016/j.hrthm.2021.04.017.

[33] I. Klem et al. "Assessment of myocardial scarring improves risk stratification in patients evaluated for cardiac defibrillator implantation". In: *Journal of the American College of Cardiology* 60.5 (2012), pp. 408–420. DOI: 10.1016/j.jacc.2012.02.070.

[34] J. K. Shade et al. "Preprocedure Application of Machine Learning and Mechanistic Simulations Predicts Likelihood of Paroxysmal Atrial Fibrillation Recurrence Following Pulmonary Vein Isolation". In: *Circulation: Arrhythmia and Electrophysiology* 13.7 (2020), e008213. DOI: 10.1161/CIRCEP.119.008213.

[35] S. Ogbomo-Harmitt et al. "Exploring Interpretability in Deep Learning Prediction of Successful Ablation Therapy for Atrial Fibrillation". In: *Medical Imaging with Deep Learning* (2022). DOI: 10.13140/RG.2.2.32298.54724.

[36] E. Lluch-Alvarez et al. "A multi-modal computer model of the heart can predict therapy outcome in cardiac resynchronization therapy (CRT)". In: *Journal of the American College of Cardiology* 75.11, Supplement 1 (2020), p. 846. DOI: https://doi.org/10.1016/S0735-1097(20)31473-X.

[37] A.F. Huxley A.L. Hodgkin. "A quantitative description of membrane current and its application to conduction and excitation in nerve". In: *The Journal of Physiology* 117.4 (1952), pp. 500–544. URL: PMCID:%20PMC1392413.

[38] K. Ten-Tusscher and A. Panfilov. "Alternans and spiral breakup in a human ventricular tissue model". In: *American Journal of Physiology-Heart and Circulatory Physiology* 291.3 (2006), H1088–H1100. DOI: 10.1152/ajpheart.00109.2006.

[39] T. O'Hara et al. "Simulation of the Undiseased Human Cardiac Ventricular Action Potential: Model Formulation and Experimental Validation". In: *PLOS Computational Biology* 7 (2011), pp. 1–29. DOI: 10.1371/journal.pcbi.1002061.

[40] G. Plank et al. "From mitochondrial ion channels to arrhythmias in the heart: computational techniques to bridge the spatio-temporal scales". In: *Philosophical Transactions of the Royal Society A: Mathematical, Physical and Engineering Sciences* 366.1879 (2008), pp. 3381–3409. DOI: 10.1098/rsta.2008.0112.

[41] E. A. Heindenreich et al. "Adaptive Macro Finite Elements for the Numerical Solution of Monodomain Equations in Cardiac Electrophysiology". In: *Annals of Biomedical Engineering* 38 (2010), pp. 2331–2345. DOI: https://doi.org/10.1007/s10439-010-9997-2.

[42] G. Houzeaux et al. "High Performance Computational Mechanics". In: *BSC-CNS* (2004).

[43] G. Plank et al. "The openCARP Simulation Environment for Cardiac Electrophysiology". In: *BioRxiv* (2021).

[44] F. B. Sachse. "Computational Cardiology". In: *Springer* (2004).

[45] H. Zhu et al. "Facilitating arrhythmia simulation: the method of quantitative cellular automata modeling and parallel running". In: *Biomedical Engineering Online* 3.29 (2004). DOI: https://doi.org/10.1186/1475-925X-3-29.

[46] D. Serra et al. "An Automata-Based Cardiac Electrophysiology Simulator to Assess Arrhythmia Inducibility". In: *Mathematics* 10.8 (2022), p. 1293. DOI: https://doi.org/10.3390/math10081293.

[47] D. Streeter et al. "Fiber orientation in the canine left ventricle during diastole and systole". In: *Circulation research* 24.3 (1969), pp. 339–347. DOI: 10.1161/01.res.24.3.339.

Appendix

	Induced VT on EPS							No VT on EPS						No EPS	
	P1	P2	P3	P4	P5	P6	P12	P7	P9	P11	P13	P14	P15	P8	P10
Clinical characteristics															
Sex (M/F)	M	M	M	M	M	M	M	M	M	M	F	M	M	M	M
Age (years)	84	70	61	49	81	53	68	63	69	60	75	56	72	50	70
LVEF (%)	28	35	32	35	25	36	37	57	59	54	43	60	39	55	47
Scar characterization															
Scar mass (g)	47.5	17.9	57.1	106.5	32.5	16.8	29.5	18.5	9.6	10.1	17.1	10.1	28.4	4.7	36.8
BZ mass (g)	42.2	13.1	34.2	65.7	24.3	13.3	21.4	13.7	8.4	7.2	8.1	8.0	21.9	3.4	24.2
CZ mass (g)	5.1	4.8	22.9	40.7	8.2	3.5	8.0	4.8	1.1	2.8	9.0	2.0	6.4	1.3	12.6

Table 8: Clinical and scar characteristics of each patient.